

**Journal of Physical Oceanography**  
**Space-Time Extremes in Short-Crested Storm Seas**  
--Manuscript Draft--

<b>Manuscript Number:</b>	JPO-D-11-0179
<b>Full Title:</b>	Space-Time Extremes in Short-Crested Storm Seas
<b>Article Type:</b>	Article
<b>Corresponding Author:</b>	Francesco Fedele, Ph.D. Georgia Institute of Technology Atlanta, UNITED STATES
<b>Corresponding Author's Institution:</b>	Georgia Institute of Technology
<b>First Author:</b>	Francesco Fedele, Ph.D.
<b>Order of Authors:</b>	Francesco Fedele, Ph.D.
<b>Abstract:</b>	<p>This study develops a stochastic approach to model short-crested stormy seas as random fields both in space and time. Defining a space-time extreme as the largest surface displacement over a given sea-surface area during a storm, associated statistical properties are derived by means of the theory of Euler Characteristics of random excursion sets in combination with the Equivalent Power Storm model. As a result, an analytical solution for the return period of space-time extremes is given. Subsequently, the relative validity of the new model and its predictions are explored by analyzing wave data retrieved from NOAA buoy 42003, located in the eastern part of the Gulf of Mexico, offshore Naples, Florida. The results indicate that as the storm area increases under short-crested wave conditions, space-time extremes noticeably exceed the significant wave height of the most probable sea state in which they likely occur, and that they also do not violate Stokes-Miche type upper limits on wave heights.</p>

1  
2 **Space-Time Extremes in Short-Crested Storm Seas**

3

4

5 Francesco Fedele<sup>1</sup>

6 School of Civil and Environmental Engineering

7 and

8 School of Electrical and Computer Engineering

9 Georgia Institute of Technology, Atlanta, USA

10

---

<sup>1</sup> *Corresponding author address:* Francesco Fedele, Georgia Institute of Technology, Atlanta, Georgia USA  
E-mail: [fedele@gatech.edu](mailto:fedele@gatech.edu)

11

12

## Abstract

13

14 This study develops a stochastic approach to model short-crested stormy seas as random  
15 fields both in space and time. Defining a space-time extreme as the largest surface  
16 displacement over a given sea-surface area during a storm, associated statistical  
17 properties are derived by means of the theory of Euler Characteristics of random  
18 excursion sets in combination with the Equivalent Power Storm model. As a result, an  
19 analytical solution for the return period of space-time extremes is given. Subsequently,  
20 the relative validity of the new model and its predictions are explored by analyzing wave  
21 data retrieved from NOAA buoy 42003, located in the eastern part of the Gulf of Mexico,  
22 offshore Naples, Florida. The results indicate that as the storm area increases under short-  
23 crested wave conditions, space-time extremes noticeably exceed the significant wave  
24 height of the most probable sea state in which they likely occur, and that they also do not  
25 violate Stokes-Miche type upper limits on wave heights.

26

27

28

## 29 1. Introduction

30 One of the key elements in the analysis of long-term predictions of extreme wave crest  
31 events is the probability of exceedance of the maximum crest height  $C_{\max}$  observed at a  
32 point  $Q$  in time  $t$  during a storm. Following Borgman (1973), this probability can be  
33 expressed as

$$34 \Pr\{C_{\max} > z\} = 1 - \exp\left\{\int_0^D \frac{\ln[1 - P(z | H_s = h(t))]}{\bar{T}[h(t)]} dt\right\}, \quad (1)$$

35 where  $h(t)$  is the time series of the significant wave height  $H_s$  recorded at  $Q$ ,  $\bar{T}(h)$  is  
36 the mean zero up-crossing period,  $D$  is the storm duration and  $P(z | H_s = h)$  is the  
37 exceedance probability of the crest height  $z$  in a sea state where  $H_s = h$ . This is  
38 described reasonably well by the Rayleigh law or the Tayfun model for linear or  
39 nonlinear waves, respectively (Tayfun 1986, Tayfun and Fedele 2007, Fedele 2008,  
40 Fedele and Tayfun 2009).

41 Borgman's formulation (1) is the starting point of various statistical methods  
42 developed for predicting occurrences of extreme events in stormy seas (Krogstad, 1985;  
43 Prevosto et al., 2000; Boccotti 2000; Isaacson and Mackenzie, 1981; Guedes Soares,  
44 1989; Goda, 1999; Arena and Pavone 2006, 2009; Fedele and Arena, 2010). These  
45 assume that the effects of the sea state observed during time intervals of the short-term  
46 scales of  $T_s \sim 1-3$  hours can be accumulated to predict the wave conditions for the long-  
47 term scales of  $T_l \sim$  years. One of the drawbacks of such stochastic analyses is that in  
48 short-crested seas, surface time series gathered at a fixed point tend to underestimate the  
49 true actual wave surface maximum that can occur over a given region of area  $E_s$  around

50  $Q$ . A large crest observed in time at  $Q$  represents a maximum observed at that point, but it  
51 may not even be a local maximum in the actual crest segment of a three dimensional (3-  
52 D) wave group. The actual crest representing the global maximum occurs at another point  
53 located without or within  $E_s$ . Certainly, the elevation of the actual crest is always larger  
54 than that measured at  $Q$ . Thus, (1) underestimates the maximum wave surface height  
55  $\eta_{\max}$  attained over  $E_s$ , which is also not the highest crest height of the group, unless the  
56 area is large enough for all wave-group dynamics to develop fully. Indeed,  $\eta_{\max}$  can also  
57 occur on the region's boundaries, and this is usually the case in areas of smaller size than  
58 the average size of wave groups. Thus, wave extremes should be modeled in both space  
59 and time as maxima of random fields rather than those of random functions of time  
60 (Adler, 1981, Piterbarg 1995, Adler and Taylor, 2007). Since in 3-D random fields it is  
61 not possible to define a wave easily or unambiguously, as is possible in time series, in this  
62 work we refer to a space-time extreme as the largest surface displacement  $\eta_{\max}$  over a  
63 given sea-surface area during a storm.

64 Note that the application of such advanced stochastic theories to realistic oceanic  
65 conditions has been limited because it requires the availability of wave surface data  
66 measurements collected both in space and time, in particular directional wave spectra  
67 (Baxevani and Richlik, 2004). Only at large spatial scales, Synthetic Aperture Radar  
68 (SAR), or Interferometric SAR (INSAR) remote sensing provides sufficient resolution  
69 for measuring waves longer than 100 m (see, e.g. Marom et al., 1990; Marom et al.,  
70 1991; Dankert et al., 2003). However, it is insufficient to correctly estimate spectral  
71 properties at smaller scales. At such scales, up to date field measurements for estimating  
72 directional wave spectra are challenging or inaccurate even if a linear or two-dimensional

73 (2-D) wave probe-type arrays could be used, though expensive to install and maintain  
74 (Allender et al., 1989; O'Reilly et al., 1996). Recently, stereo video techniques have been  
75 proposed as an effective low-cost alternative for such precise measurements (Benetazzo,  
76 2006; Wanek and Wu, 2006; Fedele et al., 2011; Gallego et al. 2011, Bechle and Wu  
77 2011, de Vries et al. 2011; Benetazzo et al. 2012). Indeed, a stereo camera view provides  
78 both spatial and temporal data whose statistical content is richer than that of a time series  
79 retrieved from wave gauges. For example, Gallego et al. (2011) have estimated  
80 directional spectra by a variational variant of the Wave Acquisition Stereo System  
81 (WASS) proposed by Benetazzo (2006). Further, WASS was used by Fedele et al. (2011)  
82 to prove that in short-crested seas the maximum surface height over a given area is  
83 generally larger than that observed in time by point measurements (see also Forristall,  
84 2006). The fact that the spatial extremes are larger than those measured at a fixed point is  
85 not only because there are more waves in a spatial domain. The main reason is that fixed  
86 point measurements cannot detect true extremes in short crested seas. Theories due to  
87 Adler (1981) and Piterbarg (1995) follow from both reasons, especially from this  
88 essential difference between fixed-point versus true spatial picture. An extreme observed  
89 at a fixed probe in time in short-crested seas indicates that a wave crest section just  
90 propagated through the probe, and the probability that the actual extreme of that crest  
91 section coincides with the extreme observed in time is simply zero. It is only in long-  
92 crested seas that one can equate the extremes observed in time with the actual spatial  
93 extremes.

94

95 As pointed out by Baxevani and Richlik (2004), the occurrence of an extreme in a  
96 Gaussian field is analogous to that of a big wave that a surfer is in search and always  
97 finds. Indeed, his likelihood to encounter a big wave increases if he moves around a large  
98 area instead of waiting to be hit by it. Indeed, if he spans a large area the chances to  
99 encounter the largest crest of a wave group increase, in agreement with the findings of the  
100 recent European Union ‘MaxWave’ project (Rosenthal and Lehner 2008).

101 In this work, the main focus is on characterizing the statistical properties of space-time  
102 extremes in short-crested sea states and their long-term predictions. The paper is  
103 structured as follows. First, the essential elements of the theory of Euler Characteristics  
104 (Adler, 1981) are introduced. Then, their application is presented in the context of the  
105 Equivalent Power Storm (EPS) model of Fedele and Arena (2010). The statistical  
106 properties of space-time extremes are then derived. Further, the relative validity of the  
107 new model and its predictions are assessed by analyzing wave measurements and  
108 directional spectra retrieved from NOAA buoy 42003 (East Gulf).

109

## 110 2. Euler characteristics and extremes

111 A significant result on the geometry of multidimensional random fields follows from  
112 the so-called Euler Characteristics (*EC*) of their excursion sets (Adler 1981) and the  
113 relation to extremes. To keep the presentation simple, hereafter random fields in three  
114 dimensions or lower are considered, but the theory is valid in any dimensions (Adler and  
115 Taylor 2007). Consider a homogenous Gaussian wave field  $\eta(x, y, t)$  over the bounded  
116 space-time volume  $\Omega$  with zero mean and standard deviation  $\sigma$  (see Figure 1). Here,

117 homogeneity simply means that  $\eta$  is stationary in time and homogenous in space. Thus,  
 118 the associated probability distributions at any points of the domain are the same and  
 119 Gaussian, irrespective of the domain's size. Given a threshold  $z$ , define the excursion set  
 120  $U_{\Omega,z}$  as that part of  $\Omega$  within which  $\eta$  is above  $z$ , viz.

$$121 \quad U_{\Omega,z} = \{(x, y, t) \in \Omega : \eta(x, y, t) > z\}. \quad (2)$$

122 In 3-D sets, the *EC* counts the number of connected volumetric components of the  
 123 excursion set  $U$ , minus the number of holes that pass through it, plus the number of  
 124 hollows inside. For two dimensional (2-D) random fields instead, the *EC* counts the  
 125 number of connected components minus the number of holes of the respective excursion  
 126 set. In one dimension (1-D), the *EC* simply counts the number of  $z$ -upcrossings, thus  
 127 providing their generalization to higher dimensions (Adler 1981).

128 Worsley (1996) presented various applications of *EC* theory to characterize the  
 129 anomalies in the cosmic microwave background radiation, galactic topologies and  
 130 cerebral activities in biomedical imaging (Taylor and Worsley 2007). *EC* theory is also  
 131 relevant to oceanic applications because Adler (1981) and Adler and Taylor (2007) have  
 132 shown that the probability of exceedance  $\Pr\{\eta_{\max} > z \mid \Omega\}$  that the global maximum  $\eta_{\max}$   
 133 of  $\eta$  over  $\Omega$  exceeds a threshold  $z$  depends on the domain size and it is well  
 134 approximated by the expected *EC* of the excursion set  $U_{\Omega,z}$ , provided that the threshold is  
 135 high. The expected *EC* approximation to the exceedance probability of  $\eta_{\max}$  can be  
 136 explained heuristically as follows. As  $z$  increases, the holes and hollows in the excursion  
 137 set  $U_{\Omega,z}$  disappear until each of its connected components includes just one local  
 138 maximum of  $\eta$ , and the *EC* counts the number of local maxima. For very large



139 thresholds, the  $EC$  equals 1 if the global maximum exceeds the threshold and 0 otherwise.

140 Thus,  $EC(U_{\Omega,z})$  of large excursion sets is a binary random variable with states 0 and 1,

141 and, for  $z \gg \sigma$ ,

$$142 \quad \Pr\{\eta_{\max} > z \mid \Omega\} = \Pr\{EC(U_{\Omega,z}) = 1\} = \langle EC(U_{\Omega,z}) \rangle, \quad (3)$$

143 where angled brackets denote expectation. This heuristic identity has been proved

144 rigorously to hold up to an error that is in general exponentially smaller than any of the

145 terms of the expected  $EC$  approximation, viz. (Taylor et al. 2005)

$$146 \quad \Pr\{\eta_{\max} > z \mid \Omega\} = \langle EC(U_{\Omega,z}) \rangle + O(\exp(-u^2(1 + \chi)/2)), \quad (4)$$

147 where  $u = z/\sigma \gg 1$  and the constant  $\chi > 0$ . Piterbarg (1995) also derived an asymptotic

148 expansion of the probability in (3) for large Gaussian maxima via generalized Rice

149 formulas (Rice 1945) valid for higher dimensions. In the following, we will first apply

150 the preceding results to homogenous 3-D Gaussian fields and then consider non-

151 stationary space-time extremes observed during a sea storm.

152

### 153 *a. Extremes of Gaussian Fields*

154 Consider the Gaussian field  $\eta(x, y, t)$  homogenous over the space-time volume  $\Omega$  of

155 size  $XYD$  (see Figure 1). Drawing upon Adler and Taylor (2007), define

$$156 \quad M_3(D, X, Y \mid H_s) = 2\pi \frac{D}{T} \frac{XY}{L_x L_y} \alpha_{xyr} \quad (5)$$

157 as the average number of ‘3-D waves’ within  $\Omega$ . Here,  $\bar{T}$  is the mean wave period,  $\bar{L}_x$   
158 and  $\bar{L}_y$  are the mean wave lengths along  $x$  and  $y$ , respectively. These, as well as the  
159 parameter  $\alpha_{xy}$  are all estimated from the moments of the directional spectrum of  $\eta$  (see  
160 appendix A). The probability that one of the ‘3-D waves’ exceeds the threshold  $z$  is given  
161 by

$$162 \quad P_v(z | H_s) = [16(z/H_s)^2 - 1]P(z | H_s), \quad (6)$$

163 where

$$164 \quad P(z | H_s) = \exp\left(-8\frac{z^2}{H_s^2}\right) \quad (7)$$

165 is the Rayleigh law.

166 If  $\Omega$  is not large, then the threshold  $z$  can also be exceeded on the boundary surface  
167  $S = \partial\Omega$  with probability

$$168 \quad P_s(z | H_s) = 4(z/H_s)P(z | H_s), \quad (8)$$

169 by one of the ‘2-D waves’. The average number of such occurrences is given by

$$170 \quad M_2(D, X, Y | H_s) = M_{2,v} + M_{2,h}, \quad (9a)$$

171 where

$$172 \quad M_{2,v} = \sqrt{2\pi} D \left( \frac{X}{\bar{T}\bar{L}_x} \sqrt{1 - \alpha_{xt}^2} + \frac{Y}{\bar{T}\bar{L}_y} \sqrt{1 - \alpha_{yt}^2} \right), \quad (9b)$$

173 and

$$174 \quad M_{2,h} = \sqrt{2\pi} \frac{XY}{\bar{L}_x \bar{L}_y} \sqrt{1 - \alpha_{xy}^2}. \quad (9c)$$

175 Here,  $M_{2,V}$  ( $M_{2,H}$ ) is the average number of ‘2-D waves’ that occur on the vertical  
 176 (horizontal) faces of  $\partial\Omega$ , and the parameters  $\alpha_{xt}$ ,  $\alpha_{yt}$  and  $\alpha_{xy}$  also depend upon the  
 177 directional spectrum (see appendix A).

178 The threshold  $z$  can also be exceeded along the perimeter  $P = \partial S$  of the surface  $S$ . In this  
 179 case, the number of such occurrences follows the Rayleigh law of (7). And, the average  
 180 number of ‘1-D waves’ that exceed  $u$  is given by

$$181 \quad M_1(D, X, Y | H_s) = \frac{D}{T} + \frac{X}{L_x} + \frac{Y}{L_y}. \quad (10)$$

182 There is no clear geometric criterion, such as that of zero upcrossings for 1-D waves, for  
 183 defining 2-D or 3-D waves. In simple terms, this can be thought as one of the space-time  
 184 cells in which the map of the wave surface  $\eta(x, y, t)$  can be portioned within a given  
 185 volume or area.

186 For large thresholds  $z \gg \sigma$ , the probability of exceedance of the absolute maximum  
 187  $\eta_{\max}$  of the wave surface  $\eta$  over  $\Omega$  is given by

$$188 \quad \Pr\{\eta_{\max} > z | \Omega\} = \Pr\{\eta_{\max} > z | V\} + \Pr\{\eta_{\max} > z | S\} + \Pr\{\eta_{\max} > z | P\}. \quad (11)$$

189 Here, each term on the right-hand side of the preceding equation denotes, from left to  
 190 right, the probability that  $\eta_{\max}$  is exceeded over the interior volume  $V$  of  $\Omega$ , its surface  $S$   
 191 or the perimeter  $P$ , respectively. The three terms can be derived as follows. The  
 192 probability that  $\eta_{\max}$  does not exceed  $z$  in  $V$  is equal to the probability that all the 3-D  
 193 waves in  $V$  have amplitudes less than or equal to  $z$ . If one assume the stochastic  
 194 independence among waves (which holds for large  $z$ ), then the first term in (11) can be  
 195 expressed as

196  $\Pr\{\eta_{\max} > z | V\} = 1 - \Pr\{\eta_{\max} \leq z | V\} = 1 - [1 - P_V(z | H_s)]^{M_3},$  (12)

197 and similarly for the other two terms, that is

198  $\Pr\{\eta_{\max} > z | S\} = 1 - \Pr\{\eta_{\max} \leq z | S\} = 1 - [1 - P_S(z | H_s)]^{M_2}$  (13)

199 and

200  $\Pr\{\eta_{\max} > z | P\} = 1 - \Pr\{\eta_{\max} \leq z | P\} = 1 - [1 - P(z | H_s)]^{M_1}.$  (14)

201 For  $z \gg \sigma$ , the preceding will lead to

202  $\Pr\{\eta_{\max} > z | \Omega\} \cong M_3 P_V(z | H_s) + M_2 P_S(z | H_s) + M_1 P(z | H_s),$  (15)

203 in agreement with Adler and Taylor (2007).

204

205 *b. Scale dimension of extremes*

206 A statistical indicator of the geometry of space-time extremes in the volume  $\Omega$  can be  
 207 defined as (see appendix B)

208 
$$\beta = 3 - \frac{4M_2\zeta_0 + 2M_1}{16M_3\zeta_0^2 + 4M_2\zeta_0 + M_1},$$
 (16)

209 where  $\zeta_0$  relates to the expected maximum surface height  $\bar{\eta}_{\max}$ . The parameter  $\beta$   
 210 represents a scale dimension of waves, i.e. the relative scale of a space-time wave with  
 211 respect to the volume's size. From (16) it is easily seen that  $1 \leq \beta \leq 3$ . In particular, if  
 212  $\beta = 3$  wave extremes are fully 3-D and they are expected to occur within the volume  $V$   
 213 away from the boundaries. For  $2 < \beta < 3$ , extremes intersect also the lateral surface of  $V$ .  
 214 The limiting case of  $\beta = 2$  is attained when one of the three sides  $D$ ,  $X$  or  $Y$  is null, say  
 215  $D=0$ , for example. In this case, the extreme can occur within an area  $E_s=XY$  and it is 2-D.

216 When the area's boundaries are touched by the extreme then  $1 < \beta \leq 2$ . The limiting case  
217 of 1-D extremes ( $\beta = 1$ ) occurs when the area  $E_s$  collapses to a line ( $X=0$  or  $Y=0$ ). As an  
218 example, Figure 2 shows the wave dimension  $\beta$  computed for each hourly sea state of  
219 the  $H_s$ -sequence recorded during the period 2007-2009 by NOAA buoy 42003, moored  
220 off the East Gulf, for  $D=1$  hour and squared  $E_s = 100^2 \text{ m}^2$ . Clearly, in milder or low sea  
221 states extremes are quasi 3-D since mean wavelengths ( $\sim 30$  m) and periods ( $\sim 3$  s) are  
222 much smaller than the lateral length  $L$  and duration  $D$ , respectively. As the intensity of  
223 the sea state increases, so do both the associated mean wavelengths (up to  $\sim 190$  m) and  
224 periods (up to  $\sim 12$  s) and the wave dimension reduces; at the highest sea states,  $\beta$  is  
225 roughly 2.6 and waves appear more long-crested. However, their sea states are broad-  
226 banded and modulational effects are negligible. In this case, extremes are expected to  
227 occur on the surfaces  $X-T$  or  $Y-T$  of the volume  $V$ .

228 In the following sections, (15) is extended for a random wave field  $\eta$  homogenous in  
229 space but non-stationary in time, thus providing a means of predicting the maximum  
230 value of  $\eta$  over an area during a storm under more realistic conditions. This also leads to  
231 a generalization of the Borgman model (1) for predicting space-time extremes in storm  
232 seas with dominant second-order nonlinearities. As discussed above, the eventual  
233 application of such approach requires spatial data, specifically directional spectra that can  
234 be estimated, for example via non-invasive stereo imaging techniques (Benetazzo 2006,  
235 Gallego et al. 2011; Fedele et al. 2011) or via SAR/INSAR remote sensing (see, e.g.  
236 Marom et al., 1990; Marom et al., 1991; Dankert et al., 2003).

237 *c. Space-time extremes during storms*

238 Consider the space-time volume  $\Omega$  of Figure 1, and regard  $\eta$  as the wave surface  
 239 generated by an actual storm passing through the area  $E_s=XY$  during a time interval  $D$ .  
 240 Assuming that  $\eta$  is spatially homogenous over the area but non-stationary in time,  
 241 partition  $D$  into  $J = D/\Delta t$  time intervals each centered at  $t = t_j$ , as shown in Figure 1.  
 242 Next, assume that  $\eta$  is locally or piecewise stationary in any time interval  $[t_j, t_j + \Delta t]$ ,  
 243 with  $\Delta t$  usually equal to 1 hour or so. The sea storm is then defined as a sequence of 3-D  
 244 stochastically independent  $\Delta t$ -sea states  $\Delta\Omega_j$  with piecewise time-varying mean period  
 245  $\bar{T}(t)$  and wavelengths  $\bar{L}_x(t)$  and  $\bar{L}_y(t)$ . Such parameters can be estimated from the  
 246 directional spectrum (see appendix A). The surface  $\Delta S_j$  of  $\Delta\Omega_j$  consists of four  
 247 ‘vertical’ faces aligned along the  $t$ -axis and surrounding the interior  $\Delta V_j$ . The perimeter  
 248  $\partial\Delta S_j$  consists of four ‘vertical’ segments, each of length  $\Delta t$ . With this setting in mind,  
 249 the volume  $\Omega$  is partitioned in disjoint subsets  $\Omega = S_b \cup S_L \cup V \cup S_u$ , where  $S_u$  and  
 250  $S_b$  are the upper and bottom surface areas of  $\Omega$  at  $t=0$  and  $D$ , respectively, and the  
 251 lateral surface  $S_L$  and interior volume  $V$  are given by

$$252 \quad S_L = \bigcup_{j=1,J} \Delta S_j, \quad V = \bigcup_{j=1,J} \Delta V_j. \quad (17)$$

253 The exceedance probability of the global maximum  $\eta_{\max}$  of  $\eta$  over  $\Omega$  can then be  
 254 expressed as

$$255 \quad \Pr\{\eta_{\max} > z | \Omega\} = 1 - \Pr\{(\eta_{\max} \leq z | V) \cap (\eta_{\max} \leq z | S_L) \cap$$

$$(\eta_{\max} \leq z | \partial S_L) \cap (\eta_{\max} \leq z | S_b) \cap (\eta_{\max} \leq z | S_u)\}, \quad (18)$$

256 where  $\partial S_L$  is the perimeter of  $S_L$ . Assuming stochastic independence, as  $\Delta t \rightarrow 0$ , or  
 257  $J \rightarrow \infty$ , (18) yields the extended Borgman's exceedance probability to space-time (see  
 258 appendix C for derivation)

$$259 \quad P(\eta_{\max} | E_s) > z) = 1 - \exp\left\{\int_0^D (P_1 + P_2 + P_3) dt\right\}, \quad (19)$$

260 where

$$261 \quad P_1(z | H_s = h) = \frac{\ln[1 - P(z_1 | H_s = h(t))]}{T[h(t)]}, \quad (20)$$

$$262 \quad P_2(z | H_s = h) = N_s \frac{\ln[1 - P_s(z_1 | H_s = h(t))]}{T[h(t)]}, \quad (21)$$

$$263 \quad P_3(z | H_s = h) = N_v \frac{\ln[1 - P_v(z_1 | H_s = h(t))]}{T[h(t)]}, \quad (22)$$

264 where the coefficients  $N_s$  and  $N_v$  are given in appendix A. Here, to account for second-  
 265 order nonlinearities, the linear amplitude  $z_1$  is related to the nonlinear amplitude  $z$  via  
 266 the quadratic equation  $z = z_1 + \mu z_1^2 / 2\sigma$  (Tayfun 1980,1986; Fedele and Tayfun 2009),  
 267 where  $\mu = \lambda_3 / 3$  represents an integral measure of steepness dependent on the skewness  
 268 coefficient  $\lambda_3$  of  $\eta$ .

269 Note that (19) is a normalized probability measure since  $P(\eta_{\max} | E_s > 0) = 1$ . As  $E_s \rightarrow 0$ ,  
 270 it reduces to

$$271 \quad P(\eta_{\max} > z) = 1 - \exp\left\{\int_0^D P_1 dt\right\}, \quad (23)$$

272 which is the Borgman's probability in (1) for the maximum wave crest  $C_{\max}$  observed in  
 273 time at point  $Q$ . The expected maximum  $\bar{\eta}_{\max}$  of the actual storm follows by integrating  
 274 (19) over  $z$  as

$$275 \quad \bar{\eta}_{\max} = \int_0^{\infty} P(\eta_{\max} | E_s > z) dz. \quad (24)$$

276 As  $z \rightarrow \infty$ , (19) tends asymptotically to

$$277 \quad P(\eta_{\max} | E_s > z) \rightarrow -\int_0^D (P_1 + P_2 + P_3) dt, \quad (25)$$

278 which is the extension of Adler's probability (15) to sea storms.

279 Note that the exceedance probability in (19) relies on the assumption of stochastic  
 280 independence of large waves, which holds for weakly non-Gaussian fields dominated by  
 281 second order nonlinearities, or short-crested seas considered in this work. Indeed,  
 282 realizations of maxima typically occur at times and locations typically well separated to  
 283 render them largely independent of one another in wind seas. Clearly, in long-crested sea  
 284 states the areal effects are negligible and (19) reduces to the time Borgman formulation  
 285 (1). However, in this case the wave surface is affected by nonlinear quasi-resonant  
 286 interactions and fourth-order cumulants increase beyond the Gaussian threshold if the  
 287 spectrum is narrow (see, for example, Fedele et al. 2011). To account for such deviations,  
 288 an obvious modification would be to simply replace in (1) the Rayleigh/Tayfun  
 289 distribution with Gram-Charlier (GC) type models, such as those developed by Mori and  
 290 Janssen (2006), Tayfun and Fedele (2007) or Fedele (2008). Indeed, GC models have  
 291 been shown to describe the effects of quasi-resonant interactions on the wave statistics  
 292 (see, for example, Fedele et al., 2011). However, in such long-crested sea states



293 individual waves are correlated (see for example, Janssen, 2003) and (1), even with a GC  
294 model, loses its validity and yields conservative estimates as an upper bound. The space-  
295 time stochastic model proposed herein can be extended to smoothly bridge long- and  
296 short-crested conditions. This would require taking into account the correlation between  
297 neighboring waves and it should depend upon the joint probability distribution of  
298 successive extremes (see, for example, Fedele 2005). Such a model would be beneficial  
299 for estimating extreme waves in rapid development of long-crested sea states in time.  
300 Some work on marine accidents suggests that such conditions may occur (Tamura et al.  
301 2008). The development of such a stochastic model is in progress and will be discussed  
302 elsewhere.

303

304

### 305 3. Prediction and properties of space-time extremes

306 In the following, (19) will be applied in the context of the EPS model of Fedele and  
307 Arena (2010) to predict the long-term statistics of space-time extremes, namely the  
308 largest surface elevation  $\eta_{\max}$  that can occur over the area  $E_s$  centered at point  $Q$  during a  
309 storm. To do so, consider a time interval  $\tau$  during which  $N(\tau)$  storms sweep through  $E_s$ ,  
310 and assume that the time series of significant wave heights ( $H_s$ ) at  $Q$  as well as the  
311 directional spectrum are given as measurements. Then, define a succession of storms  
312 where each storm, according to Boccotti (2000), is identified as a non-stationary  
313 sequence of sea states in which  $H_s$  exceeds 1.5 times the mean annual significant wave  
314 height at the site, and it does not fall below that threshold during an interval of time

315 longer than 12 hours (see also Arena, 2004). Given a succession of storm events in time,  
 316 each event is described as an EPS storm of duration  $b$  and peak amplitude  $a$  at, say,  
 317  $t = t_0$ . The significant wave height  $h$  varies in time  $t$  according to a power law  $h(t) \sim |t - t_0|^\lambda$   
 318 , where  $\lambda (>0)$  is a shape parameter (Fedele and Arena 2010). The EPS storm has sharp  
 319 cusps for  $0 < \lambda < 1$  and rounded peaks for  $\lambda \geq 1$ . For  $\lambda = 1$ , the ETS model of Boccotti  
 320 with linear cusps is recovered (Boccotti, 2000). It is then assumed that  $a$  and  $b$  are  
 321 realizations of two random variables, say  $A$  and  $B$ , respectively. Then, the storm peak  
 322 probability density function (pdf)  $p_A(a)$  is not fitted directly to the observed storm peak  
 323 data via ad-hoc regressions, but it follows analytically by requiring that the average times  
 324 spent by the equivalent and actual storm sequences above any threshold be identical, viz.

$$325 \quad p_A(a) = \frac{\tau}{N(\tau)} \frac{a}{\bar{b}(a)} G(\lambda, a). \quad (26)$$

326 Here, the function  $G(\lambda, a)$  (see Appendix D) depends on the exceedance distribution of  
 327 significant wave heights  $P(h) = \Pr\{H_s > h\}$  and the conditional average duration  
 328  $\bar{b}(a | E_s) = \overline{B | A = a}$ , both of which are estimated via regression. In particular, a Weibull  
 329 fit is adopted for  $P(h)$  as

$$330 \quad P(h) = \exp\left[-\left(\frac{h - h_l}{w}\right)^u\right], \quad (27)$$

331 where  $u$ ,  $w$  and  $h_l$  are regression parameters (see Fedele and Arena 2010). As a  
 332 consequence, the analytical form of the storm peak density  $p_A$  is defined via (26). For  
 333 example, for triangular storms ( $\lambda = 1$ )

334 
$$p_A(a) \sim \frac{a}{\bar{b}(a)} \frac{d^2 P}{da^2} = \frac{u}{w \bar{b}(a)} \left( \frac{a-h_l}{w} \right)^{u-1} \left[ u \left( \frac{a-h_l}{w} \right)^u + u-1 \right] \exp \left[ - \left( \frac{a-h_l}{w} \right)^u \right], \quad (28)$$

335 and  $p_A$  depends upon the Weibull parameters and the conditional  $\bar{b}(a)$ . For comparison,  
 336 both the Generalized Extreme Value (GEV) and Gumbel (G) models are used to fit the  
 337 observed storm peak data. In particular, the GEV density and cumulative distribution  
 338 function are given by

339 
$$p_{GEV}(a) = \frac{dP_{GEV}}{da}, \quad (29)$$

$$P_{GEV}(a) = \Pr\{A \leq a\} = \exp \left[ - \left( 1 + k(a - \mu) / \sigma \right)^{-1/k} \right], \quad a \geq \mu - \sigma / k,$$

340 where  $(k, \mu, \sigma)$  are the GEV parameters. For Gumbel,

341 
$$p_G(a) = \frac{dP_G}{da}, \quad (30)$$

$$P_G(a) = \Pr\{A \leq a\} = \exp \left[ - \exp \left[ - (a - \mu_G) / \sigma_G \right] \right], \quad a \geq 0,$$

342 where  $(\mu_G, \sigma_G)$  are regression parameters. Note that GEV tends to G as  $k \rightarrow 0$ .

343 The conditional storm base is estimated as follows. For large  $z$ , the probability that

344  $\eta_{\max} > z$  during an EPS storm is given by

345 
$$P\{\eta_{\max} | E_s > z; a, b\} = 1 - \exp \left\{ \frac{b}{\lambda a} \int_0^a \frac{P_1(z|h) + P_2(z|h) + P_3(z|h)}{(1-h/a)^{1-1/\lambda}} dh \right\}. \quad (31)$$

346 This follows from (19) specializing the significant wave height history  $h(t)$  to that of the

347 EPS storm (see Fedele and Arena 2010). As  $E_s \rightarrow 0$ , (31) reduces to the time-based

348 Borgman's probability (1) specialized to point estimates of the maximum crest height

349  $C_{\max} = \eta_{\max}$  in EPS storms, viz.

$$350 \quad P\{\eta_{\max} > z; a, b\} = 1 - \exp\left\{\frac{b}{\lambda a} \int_0^a \frac{P_1(z|h)}{(1-h/a)^{1-1/\lambda}} dh\right\}. \quad (32)$$

351 The expected maximum  $\bar{\eta}_{\max}(E_s)$  of the EPS storm then follows by integration as in (26).  
 352 For a given area  $E_s$ , the statistical equivalence between an actual storm and the associated  
 353 EPS is achieved by requiring that  $a$  equal the actual maximum  $H_s$  in the storm, and  $b$  is  
 354 chosen so that the expected maximum  $\bar{\eta}_{\max}$  during the storm is the same as that of the  
 355 EPS storm (Fedele and Arena, 2010). Once the  $\bar{\eta}_{\max}$  of the true storm is estimated from  
 356 data by means of (19) and (26), a good approximation of  $b$  is given by imposing the  
 357 exceedance probabilities of the actual and EPS storms to be equal at  $z = \bar{\eta}_{\max}$ , viz.

$$358 \quad P\{\eta_{\max} | E_s > \bar{\eta}_{\max}; a, b\} = P(\eta_{\max} | E_s > \bar{\eta}_{\max}). \quad (33)$$

359 From this,  $b$  follows as

$$360 \quad b(E_s, \lambda) = \lambda a \frac{\int_0^D (P_1 + P_2 + P_3) dt}{\int_0^a \frac{P_1 + P_2 + P_3}{(1-h/a)^{1-1/\lambda}} dh}, \quad \text{for } z = \bar{\eta}_{\max}. \quad (34)$$

361 It is observed that  $b$  depends upon the storm shape, but it slightly changes with the area  
 362  $E_s$  as expected, since  $b$  and the storm peak density  $p_A$  are unique temporal properties of  
 363 the given location, as a result of the assumed spatial homogeneity. Thus, hereafter  $b$  is  
 364 estimated as  $b(E_s, \lambda) \approx b(0, \lambda)$ , based on the Borgman's time-based model (32). As an  
 365 example, Figure 3 (top panel) shows one of the largest observed actual storms and the  
 366 associated EPS. In the same Figure, the exceedance probability (32) of the maximum  
 367 crest height expected in time at the buoy location is compared for both the actual and EPS  
 368 storms.

369 Given  $\lambda$ , the conditional average  $\bar{b}(a)$  at the buoy location is then described by

$$370 \quad \bar{b}(a) = b_m \exp[s_m (a - a_0)], \quad (35)$$

371 where  $b_m, s_m, a_0$  are regression parameters (Boccotti 2000).

372 Note that the EPS model depends on the measured data only via the observed  $P(h)$  and  
 373 the density  $p_A$  is estimated by way of (26) for an arbitrary  $\lambda > 0$ . As a result, the EPS  
 374 model is defined in a probabilistic setting and no further data fitting is necessary for  
 375 estimating extremes and associated statistics, which can be expressed explicitly as a  
 376 function of  $p_A$ . Indeed, the return period  $R(H_s > h)$  of an actual storm whose peak is  
 377 greater than a given threshold  $h$  can be expressed as (Fedele and Arena, 2010)

$$378 \quad R(H_s > h) = \frac{\tau}{N(\tau) \int_h^\infty p_A(a) da}. \quad (36)$$

379 This can also be derived exploiting compound Poisson processes (Tayfun 1979).

380 The return period  $R(\eta_{\max} | E_s > z)$  of an actual storm in which the maximum wave  
 381 surface height exceeds  $z$  can be derived as follows. Consider the number  $N_w(z | E_s)$  of  
 382 equivalent storms where the maximum surface elevation over  $E_s$  during the storm is  
 383 greater than  $z$ . Then,  $R(\eta_{\max} | E_s > z)$  of an actual storm is defined as that of an equivalent  
 384 storm whose global maximum  $\eta_{\max}$  exceeds  $z$ . Thus,

$$385 \quad R(\eta_{\max} | E_s > z) = \frac{\tau}{N_w(z | E_s)}, \quad (37)$$

386 where  $N_w(z)$  can be explicitly formulated by following the same logical steps as in

387 Fedele and Arena (2010). It is given by

388 
$$N_w(z | E_s) = \frac{1}{\tau} \int_z^{\infty} p_A(a) P[(\eta_{\max} | E_s > z; a, \bar{b}(a))] da . \quad (38)$$

389 Using (38), (37) is simplified further to

390 
$$R(\eta_{\max} | E_s > z) = \frac{1}{\int_z^{\infty} \frac{a}{\bar{b}(a)} G(\lambda, a) P[(\eta_{\max} | E_s > z; a, \bar{b}(a))] da} . \quad (39)$$

391 As  $E_s \rightarrow 0$ , this expression reduces to that for point measurements, i.e.  $R(\eta_{\max} > z)$  (see  
 392 Arena and Pavone, 2006), and thus yields the return period of a storm whose largest crest  
 393 height exceeds  $z$  at a given location in time. Drawing upon Fedele and Arena (2010) and  
 394 from probabilistic principles, one can also estimate the most probable value of the peak  
 395 significant wave height  $A$  of the storm during which the maximum  $\eta_{\max}$  exceeds a given  
 396 threshold, say,  $z$ , over the area  $E_s$ . Indeed, given that  $F = \{\eta_{\max} > z | E_s\}$ , the conditional  
 397 probability density function describing the relative frequency of occurrence of the  
 398 extreme event in the equivalent storm whose peak intensity  $A$  is in  $[a, a + da]$  is given by

399 
$$p_{A|F}(a; z) = \frac{p_A(a) P(\eta_{\max} | E_s = z; a, \bar{b}(a))}{\int_0^{\infty} p_A(a) P(\eta_{\max} | E_s = z; a, \bar{b}(a)) da} . \quad (40)$$

400 The conditional mean  $\mu_{A|F}(z, E_s)$  and standard deviation  $\sigma_{A|F}(z, E_s)$  are both function of  
 401  $z$  and area  $E_s$ . If the coefficient of variation  $\gamma = \sigma_{A|F} / \mu_{A|F} \ll 1$ , then an exceptionally  
 402 high surface elevation most likely occurs during a storm whose maximum significant  
 403 wave height, i.e. the storm peak  $A$ , is very close to  $\mu_{A|F}$ . Most likely this is also the  
 404 intensity of the sea state in which the expected extreme occurs. In the applications to  
 405 follow, it will be shown that theoretical predictions such as these implied by the EPS

406 models are approximately satisfied in actual storm data. Moreover, to compare the EPS  
 407 predictions with those based on GEV and G models, the return periods  $R(H_s > h)$  and  
 408  $R(\eta_{\max} | E_s > z)$  will be also estimated replacing  $p_A$  with  $p_{GEV}$  and  $p_G$ , which follow  
 409 from the storm-peak data via (29-30).

410

#### 411 4. Long-term extremes in the East Gulf

412 Hereafter, the space-time EPS model will be applied to elaborate some wave  
 413 measurements retrieved by the NOAA buoy 42003 moored west of Naples, Florida  
 414 during 1976-2009. The data indicates that the observed sea states at the buoy location are  
 415 short-crested in agreement with the analysis of Forristall (2007) (see also Forristall and  
 416 Ewans 1998). Indeed, their angular spreading  $\Delta\theta$ , estimated as in O'Reilly et al. (1996),  
 417 is in the range of  $[30^\circ-60^\circ]$ . The time series of long-term wave statistics for point  
 418 measurements have been elaborated showing that the exceedance distribution  $P(h)$  of  
 419 significant wave heights is well represented by the Weibull law (27) with parameters  
 420  $u=0.591$ ,  $w=0.201$  m and  $h_l=0$  m. Further, directional data available for the period 2000-  
 421 2009 are used to fit the wave parameters  $\bar{T}$ ,  $\bar{L}_x$  and  $\bar{L}_y$  from the hourly measured  
 422 directional spectra as

$$423 \quad \bar{T} = \gamma_T \sqrt{4H_s / g}, \quad \bar{L}_x = \gamma_x g \bar{T}^2, \quad \bar{L}_y = \gamma_y g \bar{T}^2, \quad (41)$$

424 where  $\gamma_T = 2.42$ ,  $\gamma_x = 0.171$ ,  $\gamma_y = 0.172$ . From the analysis of the estimated directional  
 425 spectra of the hourly sea states, the spectral parameters  $\alpha_{xt}$ ,  $\alpha_{xt}$  and  $\alpha_{xy}$  are on average

426 very small and can be set equal to zero, whereas  $\alpha_{\text{xyr}} \sim 0.7$  as an average. For the data at  
 427 hand, quasi-triangular storms are optimal ( $\lambda \sim 0.9$ ) (see Figure 3, top panel), and the  
 428 conditional base  $\bar{b}(a)$  can be estimated from a sequence of  $N(\tau) = 627$  storms, and it is  
 429 reported in Figure 3 (bottom panel).

430 Given  $P(h)$  and  $\bar{b}(a)$ , one can now compute the pdf  $p_A(a)$  of the storm peak intensity  
 431  $A$  from (26) and predict the return period  $R(H_s > h)$  from (36) for the NOAA buoy  
 432 42003. Figure 4 illustrates such predictions labelled as EPS. For comparison, the  
 433 predictions based on the estimates of  $p_A$  directly from the observed storm peak data  
 434 using GEV and Gumbel (G) models (cf. Eqs. 29 and 30) are also reported. Note that EPS  
 435 and G yield similar predictions, whereas GEV leads to overestimation at large  $R$ . The  
 436 associated return period  $R(\eta_{\text{max}} | E_s > z)$  of the largest surface height over a square area  $E_s$   
 437  $= L^2$ , with  $L=10^3$  m, is computed from (39) and shown in Figure 5 for EPS, GEV and  
 438 Gumbel. For comparisons, the associated ‘time’ predictions of the return period  
 439  $R(\eta_{\text{max}} > z)$  ( $E_s = 0$ ) are also shown. Clearly, the expected wave height  $\eta_{\text{max}}$  attained  
 440 over  $E_s$  is larger than that expected at given point in time. Further, as the area increases  
 441 the predictions tend to deviate from the ‘time’ Borgman’s counterpart as shown in the  
 442 right panel of Figure 6, which reports the EPS predictions of  $\eta_{\text{max}}$  as function of  $R$  over  
 443 increasing areas with  $L=10^2$ ,  $10^3$  and  $10^4$  m, respectively. Over such large areas, the  
 444 wave dimension  $\beta$  is expected to be roughly 3 [see Figure 2 for the case  $L=100$  m].  
 445 Thus, drawing upon Boccotti (2000), most likely  $\eta_{\text{max}}$  is the highest crest height of the  
 446 central wave of a group that focuses within the area. An estimate of the associated  
 447 steepness  $\varepsilon_h$  is needed to assess if the large crest violates the Stokes-Miche upper limit



448 for breaking. To do so, given  $R$  we need an estimate of the most probable value  $a_{\max}$  of  
 449 the peak significant wave height  $A$  of the storm during which such maximum  $\eta_{\max}$   
 450 exceeds  $z$ . This can be inferred using Eq. (40), which allows to predict the mean  $\mu_{A|F}$  of  
 451 the conditional pdf  $p_{A|F}(a; z)$  of  $A$  given  $F = \{\eta_{\max} > z \mid E_s = L^2\}$ . The stability bands for  
 452 such estimate proceed from the standard deviation  $\sigma_{A|F}$ . Figure 6 (center) shows the  
 453 associated ratio  $\eta_{\max} / a_{\max}$  as function of  $R$  for the predictions in the right panel of the  
 454 same figure. For the largest area considered ( $L=10^4$  m), this ratio increases to roughly 1.4  
 455 independently of  $z$ , thus significantly exceeding the predictions at a given point in time,  
 456 i.e. 0.9-1.1, in agreement with the stereo measurements of ocean waves (Fedele et al.  
 457 2011). Given  $a_{\max}$ , the expected steepness can be expressed as  $\varepsilon_h = k_h \eta_{\max}$ , where the  
 458 wavenumber  $k_h$  can be estimated in various ways. For example, one can extract its value  
 459 from the actual wave profile if available. Equivalently, the theory of quasi-determinism  
 460 (Boccotti 2000, Fedele and Tayfun 2009) suggests that a large crest at focusing tends to  
 461 assume the same shape as the spatial covariance. Specifically, one can take the  
 462 wavelength and thus the corresponding wavenumber value along the direction with the  
 463 shortest zero-crossing wavelength (Method 1). Alternatively, the period  $T_h$  of the largest  
 464 wave can be estimated from the time covariance (Boccotti, 2000), and  $k_h$  follows from  
 465 the dispersion relation as  $k_h = (2\pi / T_h)^2 / g$  (Method 2). For NOAA buoy 42003,  
 466  $T_h \sim 1.26\bar{T} = 3.33\sqrt{4H_s / g}$  is a decent fit, especially for intense sea states. The left panel  
 467 of Figure 6 reports both the expected steepness  $\varepsilon_h$  and the associated confidence intervals  
 468 as function of  $R$  (estimates from the  $T_h$ -fit). It is seen that the Stokes-Miche upper limit

469  $\varepsilon_{\max} \sim 0.44$  (Stokes 1880, Michell 1893) is not violated by large waves (see also Tayfun  
470 2008). This result clearly suggests that exceptional waves with  $\eta_{\max} / a_{\max} > 1$  can occur  
471 over larger areas. Clearly, such analysis provides evidence that exceptional waves with  
472  $\eta_{\max} / a_{\max} > 1$  can occur over larger areas. However, a more critical analysis of the  
473 breaking conditions is required, but this goes beyond the scopes of this paper.

474 Finally, to confirm the above long-term predictions the  $H_s$ -sequence of hourly sea-states  
475 recorded by NOAA buoy 42003 during the period 2007-2009 has been analyzed. In  
476 particular, the top panel of Figure 7 reports the short-term ( $D=1$  h) expected maximum  
477 surface height  $\eta_{\max} / H_s$  attained over  $E_s = XY$  ( $X=Y=10^3$  m) for each hourly sea-state.  
478 The associated  $\varepsilon_n$  (bottom panel of the same Figure) is also estimated directly from the  
479 directional spectrum using Methods 1 and 2, with differences less than 2%. Clearly,  
480 extremes of intense sea-states do not violate the Stokes-Miche upper limit in agreement  
481 with the long-term predictions of Figure 6.

## 482 5. Conclusions

483 The stochastic model developed herein extends the Borgman time-domain model (1)  
484 to space-time extremes and demonstrates the increased likelihood of large waves over a  
485 given area in short-crested seas (see also Baxevani and Richlick 2004). The proposed  
486 model was applied to several storms recorded by the NOAA buoy 42003. The results  
487 reveal that given a return period, the associated threshold  $z$  exceeded by the maximum  
488 surface height  $\eta_{\max}$  over a given area is greater than that predicted by the Borgman time-  
489 domain model. In particular, for the largest area considered ( $L=10^4$  m),  $\eta_{\max}$  exceeds 1.4

490 times the significant wave height  $a_{\max}$  of the sea state where the maximum occurs,  
491 significantly exceeding the ratio  $\eta_{\max} / a_{\max} \sim 0.9-1.1$  predicted from the Borgman model.  
492 These results are in agreement with those obtained from the recent stereo measurements  
493 by Fedele et al. (2011). In intense sea states, if the area is large enough compared to the  
494 mean wavelength, a space-time extreme most likely coincides with the crest of a focusing  
495 wave group that passes through the area. Further, estimates of the steepness of such large  
496 crests suggest that they do not violate the Stokes-Miche upper limit.

497 The present EPS model provides another ‘hand on the elephant’ for the subject of  
498 extreme waves (see, for example, Boccotti 1981, 1987, 2000, Fedele 2008, Fedele and  
499 Tayfun 2009, Fedele 2008, Gemmrich and Garrett 2008) by demonstrating that the  
500 occurrence of large waves over an area can be explained in terms of extremes in space-  
501 time. In particular, the proposed model is of relevance as a practical tool for identifying  
502 safer shipping routes, and for improving the design and safety of offshore facilities.

503 The correlation or stochastic dependence of wave extremes is not an issue for the  
504 statistics of maxima because realizations of maxima typically occur at times and locations  
505 typically well separated to render them largely independent of one another in wind seas.  
506 However, under conditions conducive to the rapid development of long-crested sea states  
507 such as those studied numerically by Tamura et al. (2011), stochastic dependence can be  
508 an important factor in analysis. In this regard, the space-time stochastic model proposed  
509 here can be extended to smoothly bridge long- and short-crested conditions by taking into  
510 account the correlation between neighboring waves (see, for example, Fedele 2005).

511

512

513

514

## APPENDIX A

515

**Wave parameters**

516 Drawing from Baxevani and Richlik (2004), the mean period and wavelengths are given

517 by

$$518 \quad \bar{T} = 2\pi \sqrt{\frac{m_{000}}{m_{002}}}, \quad \bar{L}_x = 2\pi \sqrt{\frac{m_{000}}{m_{200}}}, \quad \bar{L}_y = 2\pi \sqrt{\frac{m_{000}}{m_{020}}} \quad (\text{A1})$$

519 Here,

$$520 \quad m_{ijk} = \iint k_x^i k_y^j \omega^k W(\omega, \theta) d\omega d\theta \quad (\text{A2})$$

521 are spectral moments of the directional spectrum  $W$ .522 In (21-22) the coefficients  $N_s$  and  $N_v$  are given by

$$523 \quad N_v = 2\pi \frac{X}{L_x} \frac{Y}{L_y} \alpha_{xyt}, \quad (\text{A3})$$

$$524 \quad N_s = \sqrt{2\pi} \left( \frac{X}{L_x} \sqrt{1 - \alpha_{xt}^2} + \frac{Y}{L_y} \sqrt{1 - \alpha_{yt}^2} \right), \quad (\text{A4})$$

525 with

$$526 \quad \alpha_{xyt} = \sqrt{1 - \alpha_{xt}^2 - \alpha_{yt}^2 - \alpha_{xy}^2 + 2\alpha_{xy} \alpha_{xt} \alpha_{yt}}, \quad (\text{A5})$$

527

where

$$528 \quad \alpha_{xt} = \frac{m_{101}}{\sqrt{m_{200} m_{002}}}, \quad \alpha_{yt} = \frac{m_{011}}{\sqrt{m_{020} m_{002}}}, \quad \alpha_{xy} = \frac{m_{101}}{\sqrt{m_{200} m_{020}}}. \quad (\text{A6})$$

529

530

## APPENDIX B

531

### Scale dimension of extremes

532 Consider the maximum wave surface height  $\eta_{\max}$  over  $\Omega$ . From the associated  
533 probability of exceedance (15), the expected value  $\bar{\eta}_{\max}$  is given, according to the theory  
534 of extremes (Gumbel 1958), by

$$535 \quad \frac{\bar{\eta}_{\max}}{H_s} = \zeta_0 + \frac{\gamma_e}{16\zeta_0 - \frac{F'(\zeta_0)}{F(\zeta_0)}}, \quad (\text{B1})$$

536 where  $\gamma_e = 0.5772$  is the Euler-Mascheroni constant, the prime denotes derivative with  
537 respect to  $\zeta = z/H_s$  and the dimensionless  $\zeta_0$  satisfies

$$538 \quad F(\zeta) \exp(-8\zeta^2) = 1, \quad (\text{B2})$$

539 with

$$540 \quad F(\zeta) = 16M_3\zeta^2 + 4M_2\zeta + M_1. \quad (\text{B3})$$

541 Consider now as a reference the order statistics of  $N$  waves whose parent distribution  
542 follows an exceedance distribution of the form

$$543 \quad P(\eta | H_s > z) = (4\zeta)^{\beta-1} \exp(-8\zeta^2), \quad (\text{B4})$$

544 where the parameter  $\beta \geq 1$ . In particular, for  $\beta = 1$  (B4) reduces to the Rayleigh law (7)  
545 for 1-D waves, and for  $\beta = 2$  and 3 to the distributions  $P_S$  and  $P_V$  in (7-8) for 2-D and 3-D  
546 waves respectively. Thus,  $\beta$  is interpreted as a scale dimension of waves, i.e. the relative  
547 scale of the wave with respect to the volume's size.

548 In the following,  $\beta$  is related to the mean wavelengths and periods as well as the  
549 volume's geometry by equating the expected maximum  $\bar{\eta}_\beta$  of  $N$  'beta-waves' to the true  
550 maximum  $\bar{\eta}_{\max}$  in (B1). Indeed, from (B4) according to the theory of extremes (Gumbel,  
551 1958) the expected maximum  $\bar{\eta}_\beta$  of  $N$  'beta-waves' is given by

$$552 \quad \frac{\bar{\eta}_\beta}{H_s} = \zeta_N + \frac{\gamma_e}{16\zeta_N - \beta/\zeta_N}, \quad (\text{B5})$$

553 where from (B4),  $\zeta_N$  satisfies  $N(4\zeta)^{\beta} \exp(-8\zeta^2) = 1$ . The two expected maxima  $\bar{\eta}_\beta$   
554 and  $\eta_{\max}$  are identical if  $\beta$  and  $N$  are chosen, respectively, as

$$555 \quad \beta = 1 + \zeta_0 \frac{F'(\zeta_0)}{F(\zeta_0)} = 3 - \frac{4M_2\zeta_0 + 2M_1}{16M_3\zeta_0^2 + 4M_2\zeta_0 + M_1} \quad (\text{B6})$$

556 and

$$557 \quad N = \frac{F(\zeta_0)}{4\zeta_0} = 4M_3\zeta_0 + M_2 + \frac{M_1}{4\zeta_0}. \quad (\text{B7})$$

558 Here,  $N$  is the average number of waves of dimension  $\beta$  that occur within  $\Omega$ .

559

560

561

## APPENDIX C

562

### Derivation of $\Pr\{\eta_{\max} > z | \Omega\}$

563 In (18) assume the stochastic independence of the events  $\{\eta_{\max} \leq z | V\}$ ,  $\{\eta_{\max} \leq z | S_L\}$ ,

564  $\{\eta_{\max} \leq z | \partial S_L\}$ ,  $\{\eta_{\max} \leq z | S_b\}$  and  $\{\eta_{\max} \leq z | S_u\}$  (valid for large  $z$ ). Then the

565 probability of exceedance can be rewritten as

$$\begin{aligned}
566 \quad & \Pr\{\eta_{\max} > z \mid \Omega\} = 1 - \Pr\{\eta_{\max} \leq z \mid V\} \cdot \Pr\{\eta_{\max} \leq z \mid S_L\} \cdot \Pr\{\eta_{\max} \leq z \mid \partial S_L\} \cdot \\
& \Pr\{\eta_{\max} \leq z \mid S_b\} \cdot \Pr\{\eta_{\max} \leq z \mid S_u\}. \tag{C1}
\end{aligned}$$

567 Further, the last two terms on the right-hand side can be set equal to 1, assuming that the  
568 significant wave height is null or small in the beginning and at the end of the storm (  
569  $M_{2,H} = 0$  in (9)). This simplifies (C1) to

$$570 \quad \Pr\{\eta_{\max} > z \mid \Omega\} = 1 - \Pr\{\eta_{\max} \leq z \mid V\} \cdot \Pr\{\eta_{\max} \leq z \mid S_L\} \cdot \Pr\{\eta_{\max} \leq z \mid \partial S_L\}. \tag{C2}$$

571 Here, the terms on the right-hand side can now be formulated a la ‘*Borgman*’ as in (12-  
572 14) assuming the stochastic independence of the sea-state events, namely

$$573 \quad A_j = \{\eta_{\max} \leq z \mid \Delta V_j\}, \quad B_j = \{\eta_{\max} \leq z \mid \Delta S_j\}, \quad C_j = \{\eta_{\max} \leq z \mid \partial \Delta S_j\}. \tag{C3}$$

574 As a result,

$$575 \quad \Pr\{\eta_{\max} \leq z \mid V\} = \Pr\left\{\bigcap_{j=1, J} A_j\right\} = \prod_{j=1}^J [1 - P_V(z_1 \mid H_s = h_j)]^{M_3(\Delta t, X, Y \mid H_s = h_j)}, \tag{C4}$$

$$576 \quad \Pr\{\eta_{\max} \leq z \mid S_L\} = \Pr\left\{\bigcap_{j=1, J} B_j\right\} = \prod_{j=1}^J [1 - P_S(z_1 \mid H_s = h_j)]^{M_{2,V}(\Delta t, X, Y \mid H_s = h_j)}, \tag{C5}$$

577 and

$$578 \quad \Pr\{\eta_{\max} \leq z \mid \partial S_L\} = \Pr\left\{\bigcap_{j=1, J} C_j\right\} = \prod_{j=1}^J [1 - P(z_1 \mid H_s = h_j)]^{M_1(\Delta t, 0, 0, H_s = h_j)}. \tag{C6}$$

579 where  $h_j = h(t_j)$ , and  $P_V$ ,  $P_S$  and  $P$  follow from (6),(8) and (7) as the probabilities that  
580 a ‘3-D wave’, ‘2-D wave’ and ‘1-D wave’ has an amplitude larger than  $z$  in  $\Delta V_j$ ,  $\Delta S_j$   
581 and along its perimeter  $\partial \Delta S_j$ , respectively (see Figure 1). The linear amplitude  $z_1$  is

582 related to the nonlinear amplitude  $z$  via the quadratic equation  $z = z_1 + \mu z_1^2 / 2\sigma$ , where  
 583  $\mu$  is an integral measure of steepness (Tayfun 1980, Fedele and Tayfun 2009).

584 Taking the limit of  $\Delta t \rightarrow 0$ , or  $J \rightarrow \infty$  in (C3-C6) yields the extended Borgman's  
 585 exceedance probability (19) to space-time.

586

## 587 APPENDIX D

### 588 Function $G(\lambda, a)$

$$589 \quad G(\lambda, a) = \begin{cases} \frac{\sin(\pi/\lambda)}{\pi\lambda} \int_1^\infty \frac{d^2 P}{dz^2} \Big|_{a,x} (x-1)^{-1/\lambda} dx, & \lambda > 1 \\ \frac{d^2 P}{da^2}, & \lambda = 1 \\ \frac{(-1)^n a^n}{n!} \frac{\sin(\pi\xi)}{\pi\xi} \int_1^\infty \frac{d^{n+2} P}{dz^{n+2}} \Big|_{a,x} (x-1)^{-\mu} dx, & \lambda = \frac{1}{n+\xi} < 1, \end{cases} \quad (\text{D1})$$

590 with (integer)  $n > 1$  and  $0 < \xi < 1$ . If  $\lambda = 1/n$  is rational, i.e.  $\xi = 0$ , then from (D1),

$$591 \quad G(\lambda, a) = -\frac{(-1)^n a^n}{n!} \frac{d^{n+1} P}{da^{n+1}}. \quad (\text{D2})$$

592

## 593 References

- 594 Adler, R.J., 1981: *The Geometry of Random Fields*. New York: John Wiley, 1-275.  
 595 Adler, R.J., 2000: On excursion sets, tube formulae, and maxima of random fields.  
 596 *Annals of Applied Probability*, **10**, 1-74.



597 Adler, R.J., and J.E. Taylor, 2007: *Random fields and geometry*. Springer Monographs in  
598 Mathematics Springer, New York, 454 p.

599 Allender, J., Audunson, T., Barstow, S.F., Bjerken, S.H., Krogstad, E., Steinbakke, P.,  
600 Vartdal, L., Borgman, L.E., and C. Graham, 1989: The WADIC project: A  
601 comprehensive field evaluation of directional wave instrumentation. *Ocean Eng.* **16**,  
602 505–536.

603 Arena, F., 2004: On the prediction of extreme sea waves, Chapter 10 of the book  
604 ‘*Environmental Sciences and Environmental Computing*’, Vol II, (EnviroComp  
605 Institute, Fremont, California, USA), 1-50.

606 Arena, F., and D. Pavone, 2006: The return period of non-linear high wave crests. *J.*  
607 *Geophys. Res.*, **111**, C08004, doi:10.1029/2005JC003407.

608 Arena, F., and D. Pavone 2009: A generalized approach for the long-term modelling of  
609 extreme sea waves. *Ocean Modelling*, **26**, 217-225.

610 Battjes, J. A., 1970: Long term wave height distribution at seven stations around the  
611 British Isles. *Report A44 National Oceanographic Institute*, Wormley U.K.

612 Baxevani, A., and I. Richlik, 2004: Maxima for Gaussian seas. *Ocean Eng.*, **33**(7), 895-  
613 911.

614 Bechle, A.J. and C.H. Wu, 2011: Virtual wave gauges based upon stereo imaging for  
615 measuring surface wave characteristics. *Coastal Engineering*, **58**(4), 305-316.

616 Benetazzo, A., 2006: Measurements of short water waves using stereo matched image  
617 sequences. *Coastal Engineering*, **53**, 1013-1032.

618 Benetazzo, A., Fedele F., Gallego G., Shih P.-C. and A. Yezzi 2012: Offshore stereo  
619 measurements of gravity waves. *Coastal Engineering*, **64**, 127-138.

620 Boccotti, P., 1981: On the highest waves in a stationary Gaussian process. *Atti Acc.*  
621 *Ligure di Scienze e Lettere*, **38**, 271-302.

622 Boccotti, P., 1997: A general theory of three-dimensional wave groups. *Ocean Eng.*, **24**,  
623 265-300.

624 Boccotti, P., 2000: *Wave mechanics for ocean engineering*. Elsevier Science, 1-496.

625 Borgman, L. E., 1970: Maximum wave height probabilities for a random number of  
626 random intensity storms. *Proc. 12<sup>th</sup> Inter. Conf. Coastal Eng. ASCE*, 53-64.

627 Borgman, L. E., 1973: Probabilities for the highest wave in a hurricane. *J. Waterway,*  
628 *Port, Coast.and Ocean Eng.*, **99**, 185-207.

629 Cardone, V.J., R.E. Jensen, D.T. Resio, V.R. Swail, and A.T. Cox, 1996: Evaluation of  
630 Contemporary Ocean Wave Models in Rare Extreme Events: The “Halloween Storm”  
631 of October 1991 and the “Storm of the Century” of March 1993. *J. Atmospheric and*  
632 *Oceanic Technology* , **13**, 198–230.

633 Dankert, H., Horstmann, J., Lehner, S., and W.G. Rosenthal, 2003: Detection of wave  
634 groups in SAR images and radar image sequences. *IEEE Transactionson Geoscience and*  
635 *Remote Sensing*, **41**, 1437-1446.

636 de Vries, S., Hill, D.F., de Schipper, M.A., and M.J.F. Stive, 2011: Remote sensing of  
637 surf zone waves using stereo imaging. *Coastal Engineering*, **58**(3), 239-250.

638 Fedele, F., 2005: Successive wave crests in Gaussian seas. *Probabilistic Engineering*  
639 *Mechanics*, 20(4):355-363.

640 Fedele, F., 2008: Rogue Waves in Oceanic Turbulence. *Physica D*, **237**(14-17):2127-  
641 2131

642 Fedele F. and M.A. Tayfun, 2009: On nonlinear wave groups and crest statistics. *J. Fluid*

643 *Mech.*, **620**, 221-239

644 Fedele, F. and F. Arena, 2010: The equivalent power storm model for long-term  
645 predictions of extreme wave events. *J. Phys. Oceanog.*, **4**, 1106-1117.

646 Fedele F, Cherneva Z, Tayfun MA. and Guedes Soares C. 2010. NLS invariants and  
647 nonlinear wave statistics. *Physics of Fluids*, **22**, 036601

648 Fedele F., Gallego G., Benetazzo A., Yezzi A., Sclavo M., Bastianini M. and L. Cavaleri,  
649 2011: Euler Characteristics and Maxima of Oceanic Sea States. *Journal Mathematics  
650 and Computers in Simulation*, **82**(6),1102-1111

651 Fedele F., Benetazzo A. and G.Z. Forristall, 2011: Space-time waves and spectra in the  
652 Northern Adriatic Sea via a Wave Acquisition Stereo System. *30th ASME Int. Conf.  
653 Offshore Mechanics and Arctic Engng*, Rotterdam, The Netherlands, paper OMAE2011-  
654 49924

655 Ferreira, J. A., and C. Guedes Soares 2000: Modelling distributions of significant wave  
656 height. *Coastal Eng.*, **40**, 361–374.

657 Forristall, G.Z., 2000: Wave crest distributions: Observations and second order theory. *J.  
658 Phys. Oceanogr.*, **30**, 1931-1943.

659 Forristall, G.Z., 2006: Maximum wave heights over an area and the air gap problem. *25th  
660 ASME Int. Conf. Offshore Mechanics and Arctic Engng*, Hamburg, Germany, paper  
661 OMAE2006-92022

662 Forristall, G.Z., 2007: Wave Crest Heights and Deck Damage in Hurricanes Ivan, Katrina  
663 and Rita. *Offshore Technology Conference*, Houston, Texas, paper OTC 18620

664 Forristall, G. Z., and Ewans, K. C., 1998: Worldwide Measurements of Directional Wave  
665 Spreading. *Journal of Atmospheric & Oceanic Technology*, **15**(2), 440-469.

666 Gallego G., Yezzi A, Fedele F. and A. Benetazzo, 2010: A Variational Stereo Algorithm  
667 for the 3-D reconstruction of ocean waves. *IEEE Transactions on Geoscience and*  
668 *Remote Sensing*, **49** (11), 4445-4457

669 Gemmrich, J.R, and C. Garrett, 2008: Unexpected Waves, *J. Physical Oceanography*, **38**,  
670 2330-2336.

671 Goda, Y., 1999: *Random seas and Design of Maritime Structures*. World Scientific, 443 p.

672 Guedes Soares, C., 1989: Bayesian prediction of design wave height. *Reliability and*  
673 *Optimization of Structural System '88*. Springer-Verlag, 311-323.

674 Gumbel, E. J., 1958: *Statistics of Extremes*. New York: Columbia University Press, 1-  
675 373.

676 Haver, S., 1985: Wave climate off northern Norway. *Appl. Ocean Res.*, **7**(2), 85– 92.

677 Isaacson M. and N.G. Mackenzie, 1981: Long-term distributions of ocean waves: a  
678 review. *J. Waterway, Port, Coastal Ocean Eng.*, **107**, 93-109.

679 Janssen, P.A.E.M., 2003: Nonlinear Four-Wave Interactions and FreakWaves. *J. Phys.*  
680 *Oceanogr.*, **33**, 863-884.

681 Krogstad, H.E., 1985: Height and period distributions of extreme waves. *Appl. Ocean*  
682 *Res.*, **7**,158-165.

683 Longuet-Higgins, M. S., 1952: On the statistical distribution of the heights of sea waves.  
684 *J. Mar. Res.*, **11**, 245-266.

685 Marom, M., Goldstein, R.M., Thornton, E.B., and L. Shemer, 1990: Remote sensing  
686 of ocean wave spectra by interferometric synthetic aperture radar. *Nature* **345**, 793-  
687 795.

688 Marom, M., Shemer L., and E.B. Thornton, 1991: Energy density directional spectra  
689 of nearshore wavefield measured by interferometric synthetic aperture radar. *J.*  
690 *Geophys. Res.*, **96**, 22125-22134.

691 Michell, J. H., 1893: On the highest waves in water. *Philos. Mag.*, 5, 430–437.

692 Mori N. and PAEM Janssen, 2006: On kurtosis and occurrence probability of freak  
693 waves. *J. Phys. Oceanogr.*, **36(7)**, 1471-1483.

694 O'Reilly, W.C., Herbers, T.H.C., Seymour, R.J., and R.T. Guza, 1996: A comparison of  
695 directional buoy and fixed platform measurements of Pacific swell. *J. Atmos. Ocean*  
696 *Technol.*, **13**, 231-238.

697 Piterbarg, V., 1995: *Asymptotic Methods in the Theory of Gaussian Processes*. AMS ser.  
698 *Translations of Mathematical Monographs*, **148**, 1-205.

699 Prevosto, M., H.E., Krogstad, and A. Robin, 2000: Probability distributions for  
700 maximum wave and crest heights. *Coastal Eng.*, **40**, 329-360.

701 Rice, S. O., 1944: Mathematical analysis of random noise. *Bell Syst. Tech. J.*, **23**, 282-  
702 332.

703 Rice, S. O., 1945: Mathematical analysis of random noise. *Bell Syst. Tech. J.*, **24**, 46-156.

704 Sobey R.J. and L.S. Orloff, 1999: Intensity-duration-frequency summaries for wave  
705 climate. *Coastal Eng.*, **36**, 37-58.

706 Stokes, G. G., 1880: Considerations relative to the greatest height of oscillatory  
707 irrotational waves which can be propagated without change of form. *On the Theory of*  
708 *Oscillatory Waves*, Cambridge University Press, 225–229.

709 Tamura, H., Waseda, T. and Y. Miyazawa, 2009: Freakish sea state and swell-windsea  
710 coupling: Numerical study of the Suwa-Maru incident. *Geophysical Research Letters*, **36**,  
711 L01607.

712 Tayfun, M.A., 1979: Joint Occurrences in Coastal Flooding, *J. Wtrway., Port, Coast.*  
713 *and Ocean Engineering, ASCE* , **105**(WW2) , 107-123

714 Tayfun, M.A., 1980: Narrow band nonlinear sea waves. *J. Geophys.Res.*, **85** (C3), 1548–  
715 1552

716 Tayfun, M.A. 1986: On narrow-band representation of ocean waves. Part I: Theory. *J.*  
717 *Geophys. Res.*, **1**(C6):7743-7752

718 Tayfun, M.A, 2008: Distributions of Envelope and Phase in Wind Waves, *J. Physical*  
719 *Oceanography*, **38**, 2784-2800.

720 Tayfun, M.A., and F. Fedele, 2007: Wave-height distributions and nonlinear effects.  
721 *Ocean Engineering*, **34**(11-12),1631-1649

722 Taylor, J., A. Takemura, and R. Adler, 2005: Validity of the expected Euler characteristic  
723 heuristic. *Ann. Prob.*, **33**(4),1362-1396.

724 Wanek, J.M., and C.H. Wu, 2006: Automated trinocular stereo imaging system for three-  
725 dimensional surface wave measurements. *Ocean Engineering*, **33**(5-6), 723-747.

726 Worsley, K.J., 1996: The geometry of random images. *CHANCE*, **9**(1), 27-40.

727 Rosenthal W. and S. Lehner, 2008: Rogue Waves: Results of the MaxWave Project. *J.*  
728 *Offshore Mech. Arct. Eng.* **130**(2), 021006, doi:10.1115/1.2918126

729

730

731

732

733

734

735

736

## 737 **List of Figures**

738 FIG. 1. Sketch illustrating definitions relevant to the space-time volume  $\Omega$  .

739

740 FIG. 2. Wave dimension  $\beta$  of each hourly sea-state of the  $H_s$ -sequence recorded by  
741 NOAA buoy 42003 during 2007-2009 ( $D=1$  h,  $X=Y=100$  m).

742

743 FIG. 3. NOAA buoy 42003: (top) shape and exceedance probability of the maximum  
744 time crest height  $C_{\max}$  of the observed actual storm and the associated EPS storm;  
745 (bottom) duration of EPS storms and conditional base regression  $\bar{b}(a)$  from Eq. (40)  
746 (regressions parameters  $b_m=86.5$  h,  $s_m=-0.13$  m<sup>-1</sup> and  $a_0=2.22$  m).

747

748 FIG. 4. NOAA buoy 42003: predicted return period  $R(H_s > h)$  estimated with Gumbel  
749 (G), GEV and EPS models (Gumbel parameters:  $\mu_G=-2.007$  m,  $\sigma_G=2.135$  m; GEV  
750 parameters:  $\mu=2.656$  m,  $\sigma=0.422$  m,  $k=0.353$ , Weibull parameters for EPS:  $u=0.591$ ,  
751  $w=0.201$  m,  $h_l=0$ ).

752

753 FIG. 5. NOAA buoy 42003: predicted return periods  $R(\eta_{\max} > z)$  (labeled as ‘time’) and  
754  $R(\eta_{\max} | E_s > z)$  over the area  $E_s = L^2$  ( $L=10^3$  m) estimated with Gumbel (G), GEV and  
755 EPS models (regression parameters as in Figure 4).

756

757 FIG. 6. NOAA buoy 42003: (right) predicted return period  $R(\eta_{\max} | E_s > z)$  of the largest  
758 surface height  $\eta_{\max}$  over increasing areas  $E_s = L^2$  with  $L=0$  (time),  $10^2$ ,  $10^3$  and  $10^4$  m  
759 estimated with the EPS model (regression parameters as in Figure 4); (center) significant  
760 wave height  $H_s = a(\eta_{\max})$  of the most probable sea state in which  $\eta_{\max}$  occurs in terms of  
761 the ratio  $\eta_{\max} / H_s$  and (left) steepness  $\varepsilon_h$  of the associated extreme wave.

762

763 FIG. 7. NOAA buoy 42003 (East Gulf): (top) short-term expected maximum surface  
764 height  $\eta_{\max}$  over an area  $E_s = L^2$  ( $L=10^3$  m) for each hourly sea-state (period 2007-2009)  
765 in terms of the ratio  $\eta_{\max} / H_s$ ,  $H_s$  being the significant wave height, and (bottom)  
766 steepness  $\varepsilon_h$  of the associated extreme wave (dash line is the Stokes-Miche upper limit).  
767 The wave dimension  $\beta$  is  $\sim 3$  for all the analyzed sea states.

768

769

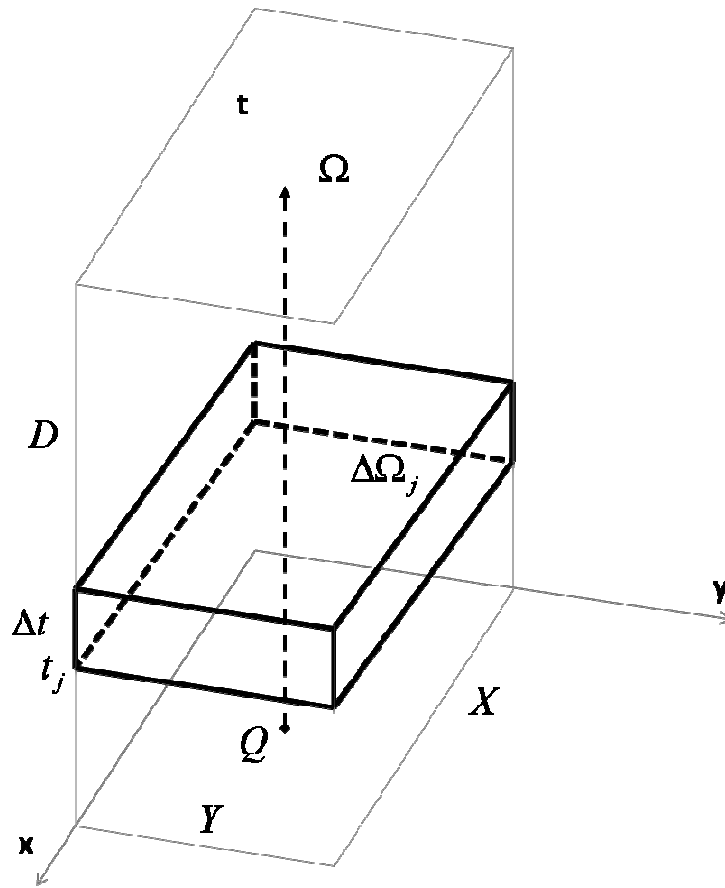
770

771

772

773





774

775

776 FIG. 1. Sketch illustrating definitions relevant to the space-time volume  $\Omega$  .

777

778

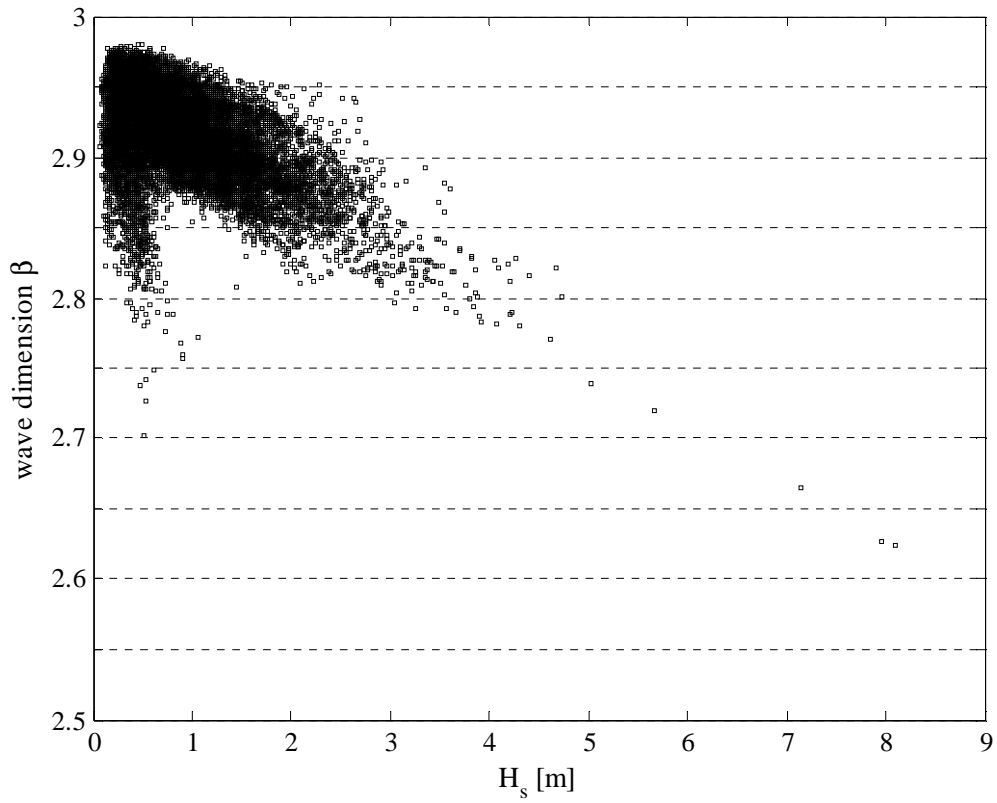
779

780

781

782

783



784

785 FIG. 2. Wave dimension  $\beta$  of each hourly sea-state of the  $H_s$ -sequence recorded by  
 786 NOAA buoy 42003 during 2007-2009 ( $D=1$  h,  $X=Y=100$  m).

787

788

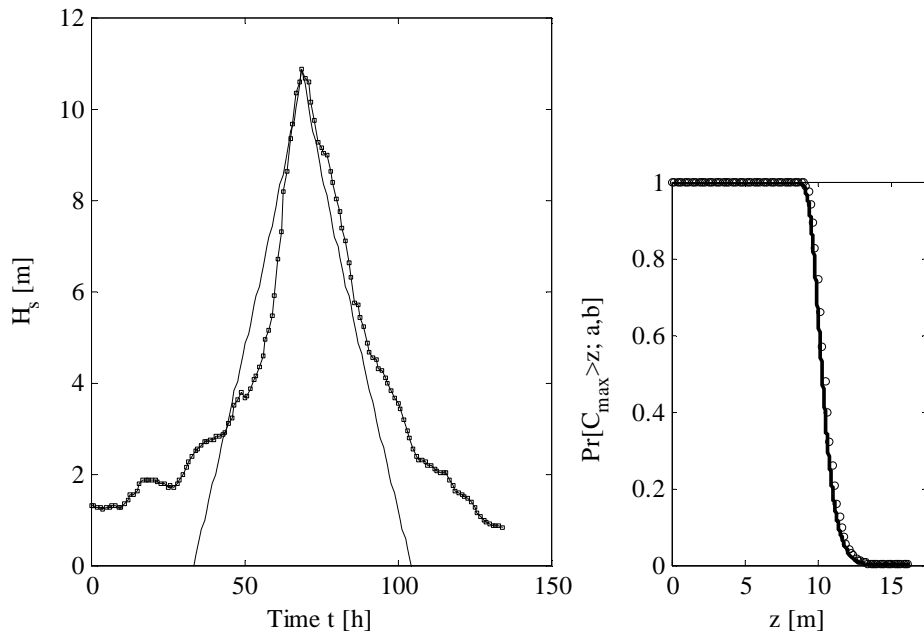
789

790

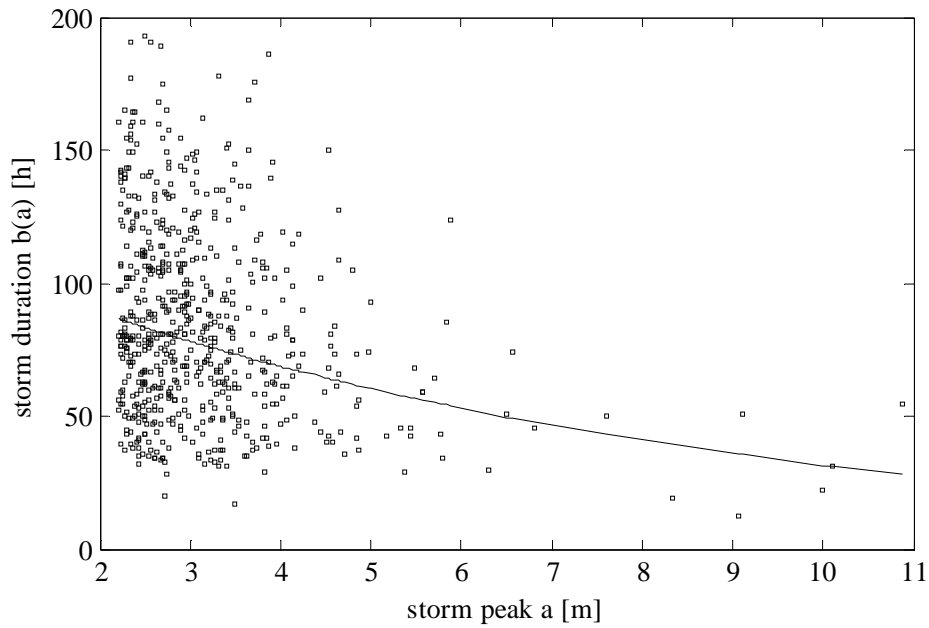
791

792

793



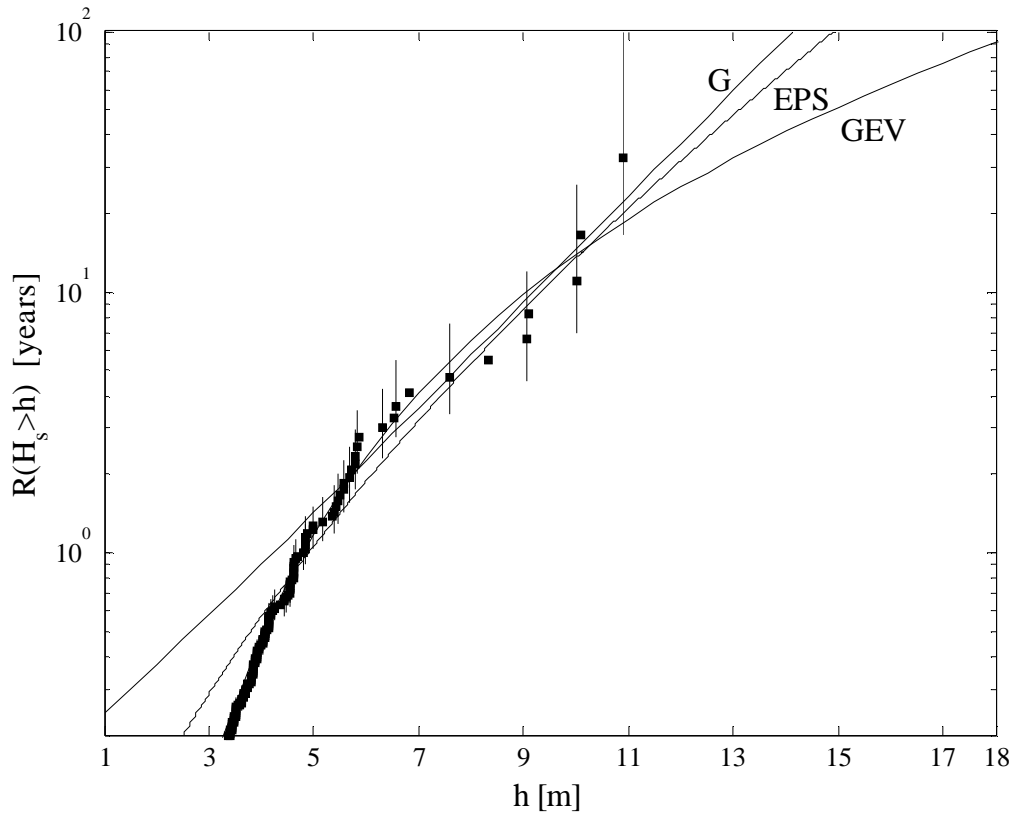
794



795

796 FIG. 3. NOAA buoy 42003: (top) shape and exceedance probability of the maximum  
 797 time crest height  $C_{\max}$  of the observed actual storm and the associated EPS storm;  
 798 (bottom) duration of EPS storms and conditional base regression  $\bar{b}(a)$  from Eq. (40)  
 799 (regressions parameters  $b_m=86.5$  h,  $s_m=-0.13$  m $^{-1}$  and  $a_0=2.22$  m).

800  
801  
802



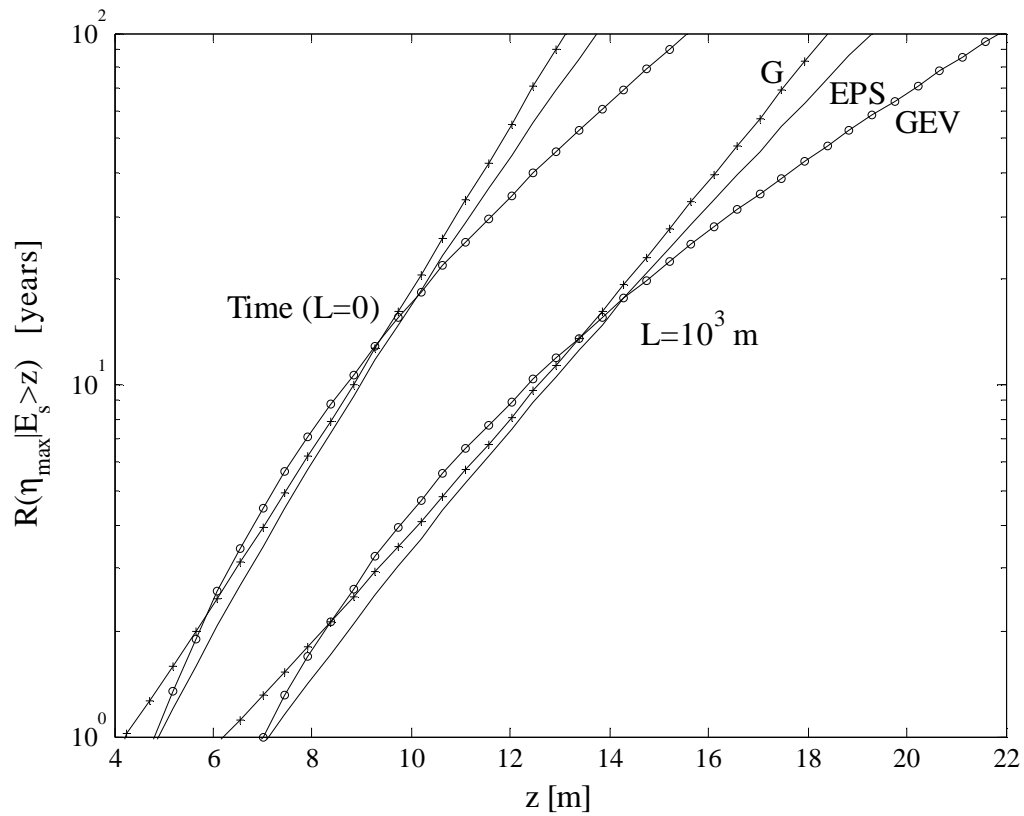
803

804 FIG. 4. NOAA buoy 42003: predicted return period  $R(H_s > h)$  estimated with Gumbel  
805 (G), GEV and EPS models (Gumbel parameters:  $\mu_G = -2.007$  m,  $\sigma_G = 2.135$  m; GEV  
806 parameters:  $\mu = 2.656$  m,  $\sigma = 0.422$  m,  $k = 0.353$ , Weibull parameters for EPS:  $u = 0.591$ ,  
807  $w = 0.201$  m,  $h_l = 0$ ).

808

809

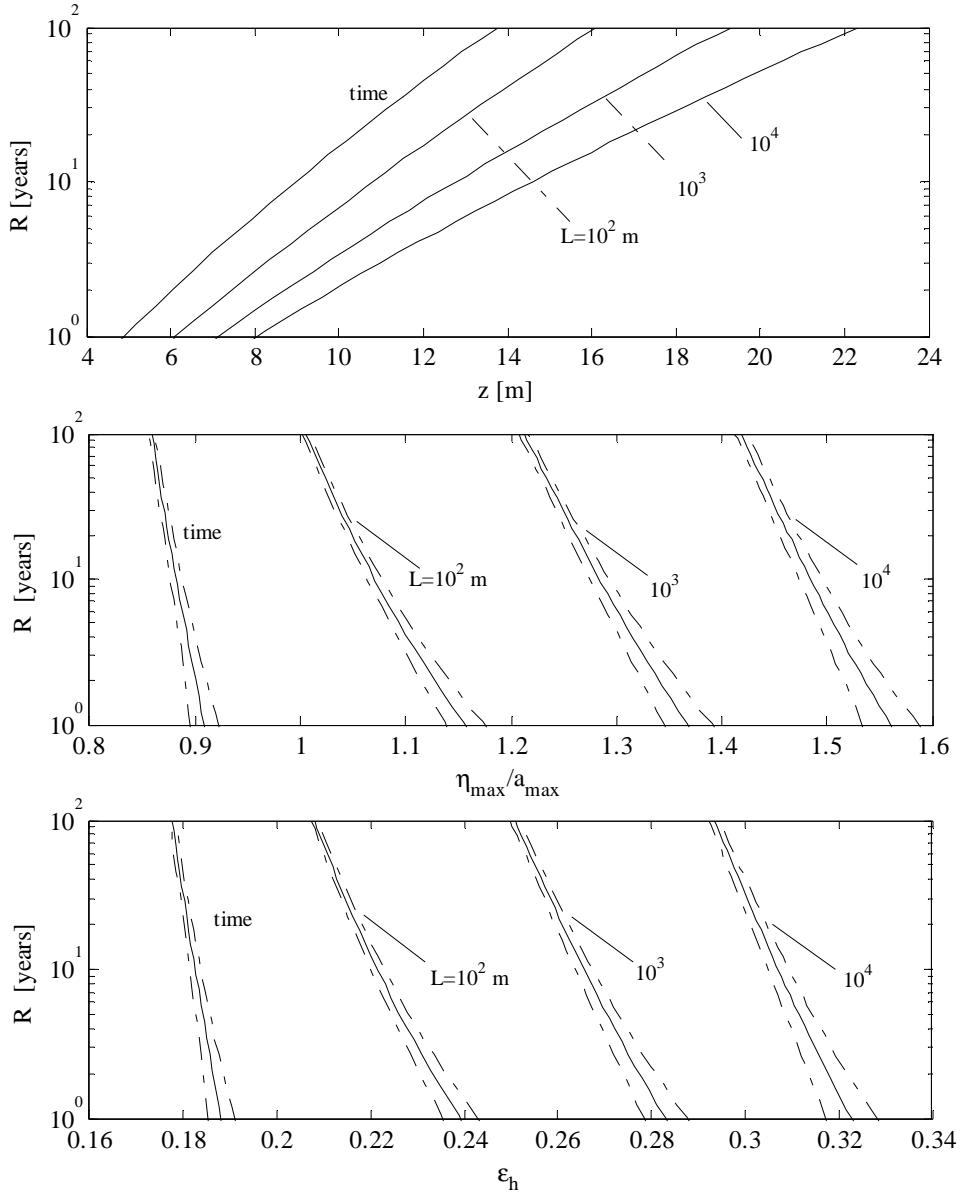
810



812

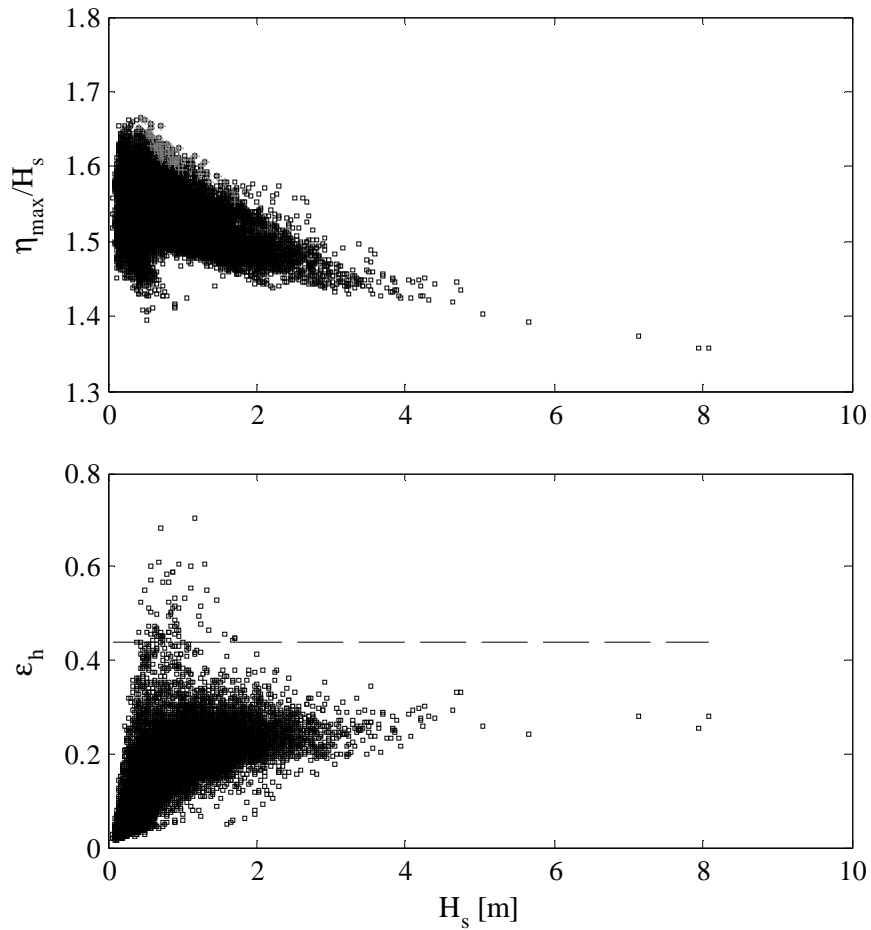
813 FIG. 5. NOAA buoy 42003: predicted return periods  $R(\eta_{\max} > z)$  (labeled as ‘time’) and  
 814  $R(\eta_{\max} | E_s > z)$  over the area  $E_s = L^2$  ( $L=10^3$  m) estimated with Gumbel (G), GEV and  
 815 EPS models (regression parameters as in Figure 4).

816



817

818 FIG. 6. NOAA buoy 42003: (right) predicted return period  $R(\eta_{\max} | E_s > z)$  of the largest  
 819 surface height  $\eta_{\max}$  over increasing areas  $E_s = L^2$  with  $L=0$  (time),  $10^2$ ,  $10^3$  and  $10^4$  m  
 820 estimated with the EPS model (regression parameters as in Figure 4); (center) significant  
 821 wave height  $H_s = a(\eta_{\max})$  of the most probable sea state in which  $\eta_{\max}$  occurs in terms of  
 822 the ratio  $\eta_{\max} / H_s$  and (left) steepness  $\epsilon_h$  of the associated extreme wave.



823

824 FIG. 7. NOAA buoy 42003 (East Gulf): (top) short-term expected maximum surface  
 825 height  $\eta_{\max}$  over an area  $E_s = L^2$  ( $L=10^3$  m) for each hourly sea-state (period 2007-2009)  
 826 in terms of the ratio  $\eta_{\max}/H_s$ ,  $H_s$  being the significant wave height, and (bottom)  
 827 steepness  $\epsilon_h$  of the associated extreme wave (dash line is the Stokes-Miche upper limit).

828 The wave dimension  $\beta$  is  $\sim 3$  for all the analyzed sea states.

829

FIG1  
[Click here to download Non-Rendered Figure: FIG1.docx](#)



FIG2  
[Click here to download Non-Rendered Figure: FIG2.eps](#)

FIG3\_bottom

[Click here to download Non-Rendered Figure: FIG3\\_bottom.eps](#)

FIG3\_top

[Click here to download Non-Rendered Figure: FIG3top.eps](#)

FIG4  
[Click here to download Non-Rendered Figure: FIG4.eps](#)

FIG5  
[Click here to download Non-Rendered Figure: FIG5.eps](#)

FIG6  
[Click here to download Non-Rendered Figure: FIG6.eps](#)

FIG7  
[Click here to download Non-Rendered Figure: FIG7.eps](#)